

To appear in *Atmosphere-Ocean*

Vol. 00, No. 00, Month 20XX, 1–29

Effects of seasonal ice coverage on the physical oceanographic conditions of the Kitikmeot Sea in the Canadian Arctic Archipelago

Chengzhu Xu

Chengzhu.Xu@dfp-mpo.gc.ca

Bedford Institute of Oceanography, Fisheries and Oceans Canada, Dartmouth, Nova Scotia, Canada

Wahad Mikhael

wahad.mikhael@ucalgary.ca

Department of Civil Engineering, University of Calgary, Calgary, Alberta, Canada

Paul G. Myers

pmyers@ualberta.ca

Department of Earth and Atmospheric Sciences, University of Alberta, Edmonton, Alberta, Canada

Brent Else

belse@ucalgary.ca

Department of Geography, University of Calgary, Calgary, Alberta, Canada

Richard P. Sims

richardpeter.sims@ucalgary.ca

Department of Geography, University of Calgary, Calgary, Alberta, Canada

Qi Zhou

qi.zhou1@ucalgary.ca

Department of Civil Engineering, University of Calgary, Calgary, Alberta, Canada

(Original manuscript received 00 Month 20XX; accepted 00 Month 20XX)

The Kitikmeot Sea is a semi-enclosed, east–west waterway in the southern Canadian Arctic Archipelago (CAA). In the present work, the ice conditions, stratification and circulation of the Kitikmeot Sea are diagnosed using numerical simulations with a $1/12^\circ$ resolution. The physical oceanographic conditions of the Kitikmeot Sea are different from channels in the northern CAA due to the existence of a substantial ice-free period each year. The consequences of such ice conditions are twofold. First, through fluctuations of external forcings, such as solar radiation and wind stress, acting directly or indirectly on the sea surface, the seasonal ice coverage leads to significant seasonal variations in both stratification and circulation. Our simulation results suggest that such variations include freshening and deepening of the surface layer, whose salinity can reach as low as 15 psu during the peak runoff season, and significantly stronger along-shore currents driven directly by the wind stress during the ice-free season. The second consequence is that the sea ice is not landfast but can move freely during the melting season. By analyzing the relative importance of thermodynamic (freezing/melting) and dynamic (ice movement) processes to the ice dynamics, our simulation results suggest that there exists a net inflow of sea ice into the Kitikmeot Sea, which melts locally each summer. The movement of sea ice thus provides a significant freshwater pathway, which contributes $\sim 14 \text{ km}^3/\text{year}$ of freshwater to the Kitikmeot Sea on average, equivalent to a third of freshwater input from runoff from the land.

KEYWORDS: Numerical Modelling, Canadian Arctic Archipelago, Kitikmeot Sea, Seasonal oceanographic conditions.

1 Introduction

The Kitikmeot Sea is a semi-enclosed, east–west waterway, located in the southern Canadian Arctic Archipelago (CAA) between Victoria Island and mainland Canada (Fig. 1a). It consists of Coronation Gulf and Queen Maud Gulf, and is bounded to the northwest by Dolphin and Union Strait and to the northeast by Victoria Strait. Coronation Gulf is relatively deeper, with the deepest part being over 300 m, whereas Queen Maud Gulf is relatively shallower with an average depth of approximately 100 m. The two gulfs are connected to each other through Dease Strait near Cambridge Bay. The existence of relatively longer ice-free seasons makes the Kitikmeot Sea the practical route for vessels traversing the Northwest Passage. Located near the centre of the Kitikmeot Sea, the coastal community of Cambridge Bay is the largest settlement in this region. In recent years, there have been significant research efforts in the Cambridge Bay area. Ocean Networks Canada (ONC) has established an underwater cabled observatory at Cambridge Bay collecting data continuously in near real-time, throughout the entire year. The Canadian High Arctic Research Station, operated by Polar Knowledge Canada, is also located at Cambridge Bay. In addition, the Kitikmeot Sea Science Study has been carried out in this region (Williams et al., 2018).

For the purpose of our analysis, we define the Kitikmeot Sea as the water body within the open boundaries indicated by the two red lines in Fig. 1(b). The surface area of the water body within these boundaries is approximately $6 \times 10^4 \text{ km}^2$, while the total volume is approximately $4 \times 10^3 \text{ km}^3$. The physical oceanographic conditions of the Kitikmeot Sea are unique, primarily due to the large amount of river runoff (relative to the size of the area) and the shallow bounding sills at both ends (less than 30 m deep at the shallowest points of both Dolphin and Union Strait and Victoria Strait). Most notably, the average salinity is much lower than that of most of the Arctic Ocean, and the circulation near the bounding sills is estuarine-like (Williams et al., 2018).

Although there have been significant research efforts in the Cambridge Bay area in recent years, comprehensive studies of the entire Kitikmeot Sea are still lacking. In particular, it is less

clear to what extent the physical oceanographic conditions of the Kitikmeot Sea vary on the seasonal time scale. The physical oceanographic conditions of the Kitikmeot Sea are different from channels in the northern CAA due to the existence of a substantial ice-free period each year. While multi-year ice covers the majority of the northern CAA, first-year ice dominates in Coronation Gulf and Dease Strait (Michel et al., 2015), though interannual variability also occurs (Howell, Derksen, Pizzolato, & Brady, 2015). The seasonal ice coverage is expected to produce significant seasonal variation in terms of both stratification and circulation, through fluctuations of external forcings such as solar radiation and wind stress, among others, acting directly or indirectly on the sea surface. The movement of sea ice during the melting season could also provide a potential freshwater pathway and affect the distribution of surface salinity. Moreover, Arctic rivers also exhibit large seasonal variation in discharge (McLaughlin, Carmack, Ingram, Williams, & Michel, 2004). These rivers are usually frozen solid for most of the year but exhibit extreme runoff events for a brief time in the summer. These runoff events could significantly affect the salinity, and hence stratification, of the Kitikmeot Sea on a relatively short time scale.

The ecology and biogeochemistry of the Kitikmeot Sea is unique within the CAA, likely a result of the unique conditions imposed by bounding sills, high freshwater content, and significant stratification. Back et al. (2021) found that the Kitikmeot Sea is perhaps the most nitrogen-depleted system in the Arctic Ocean, due largely to the inhibition of vertical mixing by stratification. This nutrient limitation significantly curtails primary production, although enhanced vertical mixing over shallow sills has been observed to create “invisible polynyas” – small areas of thin ice and high biological productivity (Dalman et al., 2019). In a survey of Arctic cod (*Boreogadus saida*) abundance in the CAA, Bouchard, Geoffroy, LeBlanc, and Fortier (2018) found a near-absence of the key forage fish in the Kitikmeot Sea, which they associated with low prey availability (in turn linked to low primary production), shallow water, and slow circulation. As a result, many marine mammals that are endemic to the CAA (e.g., beluga whales, narwhals, polar bears) are rarely observed in the region. On the other hand, the low-salinity water provides

excellent summer habitat for Arctic char, which favor estuarine conditions during their annual migration to the marine environment (Harris et al., 2020). Stratification and high freshwater content also strongly affects biogeochemistry; for example, Coronation Gulf is a key region of the CAA that is observed to act as a source of CO₂ to the atmosphere during the ice-free season (Ahmed, Else, Burgers, & Papakyriakou, 2019), likely due to strong river discharge and high summer sea surface temperature. In a rapidly changing climate, the ecosystem of the Cambridge Bay area has been under emerging pressures from environmental changes and human activities, e.g., reduced ice coverage and increased shipping activities (Falardeau-Côté, 2020).

To date, most research efforts in the Kitikmeot Sea focus on ocean observations, in which data collected tend to be sparse in space and/or time. Modelling studies, on the other hand, can provide insights into the physical oceanographic conditions on a larger spatial and temporal scale, which are essential for the better understanding of the local ecosystem, in particular carbon cycling, nutrient transport and primary production. In the present work, results of numerical simulations with a 1/12° resolution are diagnosed, in order to better understand the physical oceanographic conditions of the Kitikmeot Sea, particularly the implications of the seasonal ice coverage on the stratification and circulation. The remainder of this paper is organized as follows. The numerical model and methods of analyses are described in Sect. 2. The model is evaluated in Sect. 3 by comparing model output with available observational data. The simulation results are presented in Sect. 4, focusing on the ice conditions, stratification and ocean circulation. The implications of the physical oceanographic conditions on the local ecosystem and biogeochemistry are discussed in Sect. 5. Finally, findings of this work are summarized in Sect. 6.

2 Methods

2.a *Model description*

The numerical model used in this study is the Nucleus for European Modelling of the Ocean (NEMO) (Madec & the NEMO team, 2008) Version 3.4 coupled with the Louvain-la-Neuve Sea

Table 1. Summary of input data.

Input data	Data source	Spatial resolution	Temporal resolution
Topography	W. H. Smith and Sandwell (1997)	1 to 12 km	Not applicable
	ETOPO1 (Amante & Eakins, 2009)	1/60 degree	Not applicable
Initial conditions	GLORYS2v3 (Masina et al., 2017)	1/4 degree	Not applicable
Open boundary conditions	GLORYS2v3 (Masina et al., 2017)	1/4 degree	Monthly
Atmospheric forcings	CGRF (G. C. Smith et al., 2014)	33 km	Hourly
River discharge	Dai et al. (2009)	1 degree	Monthly
Greenland meltwater	Bamber et al. (2012)	5 km	Monthly

Ice Model (LIM) Version 2 (Hunke & Dukowicz, 1997). The model is configured for the Arctic and Northern Hemisphere Atlantic at $1/12^\circ$ resolution (ANHA12), with open boundaries located at Bering Strait and 20° S at the Atlantic Ocean. The model grid is extracted from the ORCA12 tri-polar grid (Drakkar Group, 2007), in which one of the mesh North Poles is located directly to the south of the Kitikmeot Sea. With this grid configuration, the model has the lowest resolution near the equator but the highest horizontal resolution within the Kitikmeot Sea, which is about 2 km in both zonal and meridional directions, as shown in Fig. 1(b). In the vertical direction, there are 50 levels with layer thickness smoothly increased from ~ 1 m at the surface to ~ 450 m at the bottom. Enhanced resolution is applied to the surface layer, with < 2 m vertical resolution for the top 10 m. The top 100 m is covered by 22 vertical levels, while the deepest location of the Kitikmeot Sea is covered by 30 levels. Partial steps (Bernard et al., 2006) are utilized to better resolve the ocean floor. Further detail on the ANHA12 configuration can be found in Hu, Sun, Chan, and Myers (2018).

The input data of the model are summarized in Table 1. The topography of the sea floor in the model is interpolated from bathymetry data collected by W. H. Smith and Sandwell (1997) and ETOPO1 Global Relief Model (Amante & Eakins, 2009). While these datasets are the best available datasets for the model bathymetry, the lack of small scale features might be a concern. In particular, since the model was originally set up for studying large-scale Arctic dynamics,

several narrow and shallow regions are not represented, including the southern Bathurst Inlet and the water body to the south of Kent Peninsula. Long term studies of the Kitikmeot Sea will need to carefully consider all details of the local topography.

The simulations are initialized on 1 January, 2002. The initial and open boundary conditions, including temperature, salinity, zonal and meridional velocities, sea surface height and sea ice fields, are interpolated from the $1/4^\circ$ Global Ocean Reanalysis and Simulations (GLORYS2v3) produced by Mercator Ocean (Masina et al., 2017). The atmospheric forcings, including wind stress, precipitation, air temperature, specific humidity, short-wave and long-wave radiation, are interpolated from the Canadian Meteorological Centre Global Deterministic Prediction System Reforecasts (CGRF) dataset with temporal resolution of 1 hour and spatial resolution of 33 km (G. C. Smith et al., 2014). The freshwater input from the continent is remapped from interannual monthly 1° resolution river discharge data (Dai, Qian, Trenberth, & Milliman, 2009) and 5 km resolution Greenland meltwater data (Bamber, van den Broeke, Ettema, Lenaerts, & Rignot, 2012) onto the model grid. For study periods beyond the coverage of the original datasets (i.e., since 2007 for river discharge and 2010 for Greenland meltwater), available source data from the latest years are adopted. Due to the considerable volume of the output data, the output is written out as 5-day time-averaged data.

When the model was originally set up, no tidal forcing was included. Based on the data presented in Padman and Erofeeva (2004), the mean tidal current speed is generally small in the Kitikmeot Sea (~ 1 cm/s) except for regions near shallow sills such as Victoria Strait (~ 10 cm/s). While the overall circulation is not likely to be affected dramatically, this still poses a major limitation in terms of inflow/outflow through the bounding sills, and future experiments will need to include explicit tidal forcing.

2.b *Calculations of ice thickness changes*

The ice model is coupled to the ocean model at every model time step. It calculates ice dynamics due to both thermodynamics (freezing/melting) and dynamic (transport) processes (Fichefet &

Maqueda, 1997). While these two processes occur simultaneously in the real world, they can be decoupled in the model, so that the relative importance of each of them can be better understood. In practice, we will assess the importance of each process in terms of change of ice thickness with respect to time. Let H denote the total thickness of the sea ice, the decomposition can be written as

$$\frac{dH}{dt} = \frac{d}{dt} (H_{thermal} + H_{dynamic}), \quad (1)$$

where $H_{thermal}$ and $H_{dynamic}$ denote the contribution of the thermodynamic and dynamic processes, respectively, to the overall change of ice thickness.

The fact that sea ice is not necessarily always landfast means that the movement of sea ice provides a potential pathway for freshwater transport. To quantify the net inflow of sea ice into the Kitikmeot Sea, we define the volume flux of sea ice through a particular channel cross-section, denoted by Q_{ice} , as

$$Q_{ice} = \int_a^b HC_{ice}v_{ice}ds, \quad (2)$$

where a and b are the two endpoints of the channel cross-section, C_{ice} is the ice concentration, v_{ice} is the magnitude of ice velocity perpendicular to the cross-section with positive direction pointing toward Kitikmeot Sea (so that inflow is positive and outflow is negative), and ds is defined along the cross-section. In our calculation, the two cross-sections are chosen to be within the Dolphin and Union Strait and Victoria Strait, as indicated by the red lines in Fig. 1(b).

2.c Calculations of freshwater and heat contents

Following Hu, Myers, and Lu (2019), the freshwater content (FWC) of the Kitikmeot Sea is defined as

$$FWC = \int_{z_1}^0 \frac{S_{ref} - S}{S_{ref}} dz, \quad (3)$$

where S is the salinity from model output, S_{ref} is the reference salinity which is set to be 34.8 psu, and z_1 is the lower limit of the depth level of integration which is chosen to be the 34.8 psu halocline. The freshwater content is measured by meters. Given the freshwater content, the total freshwater storage (i.e. volume) can be calculated by integrating FWC over the entire surface area of the Kitikmeot Sea, i.e.,

$$FW_{storage} = \iint_A FWC dA. \quad (4)$$

Following Myers and Ribergaard (2013), the heat content (HC) per unit area is defined as

$$HC = \rho_0 C_p \int_{z_2}^0 (T - T_{ref}) dz, \quad (5)$$

where T is the temperature from model output, T_{ref} is the reference temperature which is set to be 0°C, z_2 is the lower limit of the depth level of integration which is chosen to be 40 m below the surface, ρ_0 is the reference density which is set to be 1022 kg/m³, and C_p is the specific heat of water and is set to be 4182 J/(K kg).

3 Model evaluation

3.a Comparison to data collected by Ocean Networks Canada

The model output is compared with two sets of observational data measured in the Cambridge Bay area (Fig. 2). The first set of data is collected by Ocean Networks Canada (ONC), which has established an underwater observatory near the shore of Cambridge Bay (indicated by the star in Fig. 2) at a depth of 8 m (Duke et al., 2021). Because these data are measured in the shallow water inside a coastal bay, the small scale features are challenging for even a higher-resolution model to represent. In order for the model to represent the overall dynamics in this region, time series of model data are produced by averaging the model output over an area covering Cambridge Bay and the surrounding water (indicated by the blue box in Fig. 2), instead of a single point. We have tested different sizes and locations of the box near Cambridge Bay, and

found that the results are not sensitive to the particular sizes or locations over which the model output data are averaged. Moreover, the model data are averaged at the layer 8 m below the surface, in order to match the particular depth at which ONC's observatory is located.

The comparison between model output and data collected from ONC's observatory is shown by time series plots in Fig. 3. For both datasets, 5-day averaged values are shown. The figure suggests that the model captures the overall seasonal cycle for sea ice and water temperature reasonably well. The timing for break-up and freeze-up of sea ice in the model is consistent with observation, except for 2015 (details of the ice conditions in 2014–2015 will be discussed in Sect. 4.a). The observed ice thickness is measured in terms of ice draft by ONC and hence is slightly lower than that estimated by the model. To adjust for this difference, the original data are multiplied by 1.11 to produce the red curve in panel (a), assuming that the density of ice is roughly 90% of the density of seawater (Timco & Frederking, 1996). The temperature data also show good agreement between the model and observation, with the exception of summer 2015 where temperature estimated by the model is lower than that observed, which is likely due to the excessive summer sea ice that reduces heat input in the model.

For salinity, Panel (c) shows that from November to May the model data and observational data are similar, but some issues exist from May to November, when the salinity estimated by the model is lower than that observed from the ONC observatory. One of the reasons contributing to this difference, as discussed in the previous section, is the lack of runoff data for the model from 2007 onward, which affects the model's ability to accurately estimate the fresh water content in the water body especially in the summers. Moreover, the ONC observatory is located extremely close to the shore, but the model has limited capability of accurately representing the dynamics in this particular location. The comparison of density data is similar to that of salinity data as the density in the Arctic Ocean is determined primarily by salinity.

3.b Comparison to data collected on *RV Martin Bergmann*

From 2015 to 2018, oceanographic CTD transects were conducted annually in the Kitikmeot Sea on *RV Martin Bergmann* during the first week of August. The locations of measurements are indicated by the red dots and denoted as “R1” to “R5” in Fig. 2, and the transect that connects these locations (i.e., the “R-transect”) is indicated by the blue line. A Seabird Scientific SBE19plus CTD measuring at 5 Hz was used to make the CTD measurements except in 2016 when a RBR Concerto also measuring at 5 Hz was substituted in for the SBE19plus. Annual calibrations were completed between each field season at the Institute of Ocean Sciences (Sidney, British Columbia, Canada). The descent speed typically varied between 0.3 and 1 m/s. Measurements were interpolated down to 0.01 m and bin averaged to 0.1 m.

Figures 4 and 5 show comparison of temperature and salinity data between measurements collected at locations “R1” to “R5” and model output along the transect connecting these locations. Note that part of the difference between the model output and measurements is due to the fact that model output is averaged over a 5-day period. Fig. 4 shows that the model correctly captures the salinity at least in the surface layer (within approximately 40 m of depth), including the significant amount of surface freshwater in 2015 due to delay of ice melting in that particular year. On the other hand, in the bottom layer the model estimation of salinity is slightly higher than measured, while measurements suggest that there is no significant difference from the upper layer. Fig. 5 shows that the model estimated temperature matches the measured temperature qualitatively, except for 2015 when the model under estimates the surface temperature due to possibly excessive summer sea ice in the model. In the other years, the model slightly over estimated the extent of surface warm water and the bottom temperature.

To summarize, the comparison between model data and measurements suggests that the model is able to represent aspects of the large scale circulation and hydrography reasonably well. Some errors might be from missing or parameterized processes, issues with the initial conditions and/or forcing (such as the lack of runoff data), etc., and could be reduced as the model improves in the future.

4 Simulation results

4.a Ice conditions

The simulation results from 2011 to 2018 will be discussed in this section, where all data presented are from the model output, unless otherwise specified. The total volume of the sea ice within the Kitikmeot Sea enclosed by the boundaries indicated by the red lines in Fig. 1(b) is shown as a time series in Fig. 6. The annual volume of ice formed and melted varies from 60 to 80 km³ from year to year. Unlike the northern CAA which is ice-covered during most of the year, in the Kitikmeot Sea there is a significant ice-free period in each year, leading to greater seasonal variations in its physical oceanographic conditions. For example, the formation and melting of sea ice plays a dominant role in the seasonality of the surface freshwater process (Hu et al., 2019). Our simulation results suggest that, on average, ice concentration in the Kitikmeot Sea is at or about 100% from November to June each year, with the ice thickness reaching its maximum in May, although spatial and interannual variations exist. For the purpose of our analysis, we shall consider November to June as the ice-covered season, and July to October as the ice-free season.

Fig. 7 shows that, when averaged over ice-covered seasons from 2011 to 2018, ice thickness is over 2 m in M'Clintock Channel and reduces gradually from Queen Maud Gulf (QMG) to Coronation Gulf (CG). In Amundsen Gulf, the average ice thickness is less than 1 m. The decrease of ice thickness from M'Clintock Channel to Amundsen Gulf is consistent with previous studies of sea ice in the CAA (e.g., Haas & Howell, 2015; Michel et al., 2015), which suggested that multi-year ice (MYI) of significant concentration and thickness exists in the northern CAA and M'Clintock Channel, while Amundsen Gulf and CG is dominated by first-year ice (FYI) of less concentration and thickness. Hu et al. (2018) showed that the net production of sea ice in the CAA is due to both thermodynamic (e.g., cold temperature) and dynamical (e.g., local advection) processes, though their contribution can be either positive or negative, and that when FYI dominates thermodynamic processes play a more important role in determining the ice thickness. Along the Alaska coast, the seasonal ice melt is mainly triggered by inflow of warm

Pacific water (Shimada et al., 2006; Woodgate, Aagaard, & Weingartner, 2006). Since exchange of water (and hence the heat content) between the Kitikmeot Sea and the rest of the Arctic Ocean is relatively limited due to the existence of the bounding sills, melt in this region is likely driven by the local thermodynamic process.

Two sites, located at the deepest points of QMG (~ 125 m) and CG (~ 325 m), respectively, are selected to further study the ice conditions and their seasonal variations. These locations are indicated by the red dots in Fig. 7. A comparison of the ice conditions at these two locations is shown in Fig. 8. It is clear from this figure that QMG has a longer ice-covered period in general, and that ice thickness in QMG is larger than that in CG, especially in 2014–2015. The fluctuation of the ice conditions in QMG could be one of the reasons that the model results are different from measurements by ONC as illustrated in Fig. 3. The ONC observatory is located very close to the shore, and thus is less likely to be affected by the larger-scale ice dynamics in QMG and M’Clintock Channel. However, by analyzing data from 1980 to 2012, Michel et al. (2015) showed that there is a 20%–40% chance for MYI to be present in QMG, which is much more frequent than our model estimation from 2011 to 2018 suggested. This is most likely due to the fact that, in recent years, there has been significant decrease in the summer sea ice extent and MYI extent in the southern CAA, especially in M’Clintock Channel (Howell et al., 2013; Michel et al., 2015).

For the two study sites discussed above, ice thickness changes due to the thermodynamic and dynamic processes, as well as ice thickness changes combined from both processes, are shown in Fig. 9. It is clear from the figure that during the freezing season, which starts in December in both locations and lasts until late April in CG and mid May in QMG, change of ice thickness due to the dynamic process is approximately zero, and that the thermodynamic process plays a dominant role in determining the ice thickness in both locations. This means that most sea ice during this period is landfast ice. During the melting period which is from May to early July in CG and to late August in QMG, the thermodynamic process contributes to the majority of ice reduction. In fact, ice movement from M’Clintock Channel to QMG through Victoria Strait

is evident, since the dynamic process alone leads to an increase in the ice thickness during this period, as shown in Panel (b). In CG, on the other hand, Panel (a) shows that the dynamic process leads to a decrease of ice thickness during the same period, implying the existence of a net outflow of the sea ice. After the melting period, there is a period in which changes of ice thickness are nearly zero in CG from mid July to late September, whereas in QMG such period of time does not exist. Finally, ice thickness starts to increase due to the dynamic process in late September in CG and early September in QMG, while the local freeze-up begins due to the thermodynamic process in late October in CG and early October in QMG.

While sea ice that grows and decays in situ (i.e., due to the thermodynamic process) does not change the overall freshwater content in this region, the transport of sea ice due to the dynamic process is important for freshwater input. To quantify the net inflow of sea ice into the Kitikmeot Sea, we calculated the volume flux of sea ice through both Dolphin and Union Strait (DUS) and Victoria Strait (VS). The results are shown in Fig. 10, where positive values represent inflow while negative values represent outflow. The figure shows that, while landfast ice exists between November to May, there exists significant ice movement from May to November, with peak volume reaching $200 \text{ km}^3/\text{year}$ at VS. When a time average is taken from 2011 to 2018, the net inflow of sea ice is 24.61 km^3 per year through VS and -10.83 km^3 per year through DUS. Given the positive net inflow through VS and negative net inflow through DUS, it is clear that the direction of ice movement is generally westward, i.e., from VS to DUS. Combining the net inflow at these two open boundaries together, the total inflow of sea ice into the Kitikmeot Sea is approximately 14 km^3 per year, equivalent to approximately $1/6$ of the maximum volume of sea ice existing in the end of the freezing season, and a third of freshwater input from river runoff ($\sim 41 \text{ km}^3$ per year, Williams et al., 2018). Therefore, the fact that there is a net inflow of sea ice which melts locally each summer suggests that the movement of sea ice is a significant freshwater pathway and has an effect on surface salinity distributions in a way similar to runoff from land.

4.b Stratification

Stratification of the Kitikmeot Sea is a unique characteristic, due to the large amount of freshwater input and the existence of the shallow bounding sills. Most notably, the salinity of the Kitikmeot Sea is much lower than that of most of the Arctic Ocean. The freshwater storage of the Kitikmeot Sea is calculated using the method described in Sect. 2 and shown as a time series in Fig. 11. While interannual variability exists, the difference between maximum and minimum freshwater storage each year is 100–150 km³ in the ocean only and slightly over 50 km³ when combined with freshwater in sea ice. The sources of freshwater input include ice melted, runoff from land, and net precipitation. The contribution from the latter is relatively minor given the relatively short period of the ice-free season. On the other hand, the actual amount of freshwater input from ice melted could be more than the maximum volume of sea ice existing in the end of each freezing season, since there exists a net inflow of sea ice into the Kitikmeot Sea during the melting season, as discussed in the previous section. While a year-to-year increase of freshwater content can also be noticed in Fig. 11, it is not clear if such interannual variability is a long-term trend given the short simulation period. The interannual variability is not the focus of this paper and should be discussed in future studies when simulations are performed over a much longer time span.

The freshwater and heat contents of the Kitikmeot Sea, calculated using the method described in Sect. 2.c and averaged from 2011 to 2018, is shown in Fig. 12. To be consistent with literature of freshwater content of the Arctic Ocean (e.g., McPhee, Proshutinsky, Morison, Steele, & Alkire, 2009), the reference salinity for calculating the freshwater content is set to be $S_{ref} = 34.8$ psu. This value is larger than the maximum salinity of the Kitikmeot Sea, so that the entire water column is included in the integration. For this reason, CG has much more freshwater content than QMG, since it is much deeper in general. The average depth of freshwater content in CG is approximately 30 m, while the maximum depth can reach as much as 39 m. This value almost doubles the freshwater content per unit area in the Beaufort Gyre (Proshutinsky et al., 2019), which is significantly influenced by the Pacific water. While the Pacific water is

Table 2. Model estimation of minimum, maximum and average salinity, temperature and potential density at locations indicated by the red/cyan dots in Fig. 12 between 2011 and 2018.

Location	Dease Strait	Queen Maud Gulf	Coronation Gulf
Minimum salinity (psu)	14.5	15.2	19.9
Maximum salinity (psu)	31.0	31.5	33.0
Average salinity, upper 40 m (psu)	27.4	27.1	27.4
Average salinity, 40–150 m (psu)	29.3	30.2	29.6
Average salinity, below 150 m (psu)	N/A	N/A	32.5
Minimum temperature ($^{\circ}\text{C}$)	-1.7	-1.6	-1.9
Maximum temperature ($^{\circ}\text{C}$)	8.0	6.3	10.1
Average temperature, upper 40 m ($^{\circ}\text{C}$)	-0.4	-0.7	0.3
Average temperature, 40–150 m ($^{\circ}\text{C}$)	-0.1	-0.2	0.5
Average temperature, below 150 m ($^{\circ}\text{C}$)	N/A	N/A	-0.8
Minimum density (kg/m^3)	1011.54	1012.11	1015.90
Maximum density (kg/m^3)	1024.88	1025.27	1026.50
Average density, upper 40 m (kg/m^3)	1022.00	1021.77	1021.90
Average density, 40–150 m (kg/m^3)	1023.55	1024.27	1023.76
Average density, below 150 m (kg/m^3)	N/A	N/A	1026.10

the primary source of freshwater entering into the Arctic Ocean (Haine et al., 2015; Woodgate, Weingartner, & Lindsay, 2010), our results suggest that the Pacific water is not nearly as fresh as water in the Kitikmeot Sea. In fact, any inflow of water from the Pacific origin through either DUS or VS will decrease the freshwater content of the Kitikmeot Sea by displacing the fresher water within this region.

Fig. 12(b) shows that the surface water in CG is warmer than that in QMG in general. This is most likely due to the longer open water season in CG (Fig. 8a), and the net inflow of sea ice into QMG from M’Clintock Channel (Figs. 9–10). Note that the heat content in most areas of QMG is negative, because when time average is taken, the averaged temperature is below the reference temperature of 0°C .

Three sites, located at the deepest points of QMG and CG, respectively, and in Dease Strait

(DS) between Cambridge Bay and Kent Peninsula (“R3” in Fig. 2), are selected to further study the seasonal variation of salinity and temperature. These locations are indicated by the red/cyan dots in Fig. 12. The Hovmöller plots of the salinity and temperature at these locations are shown in Figs. 13 and 14, respectively, while several quantitative measurements are given in Table 2. Note that there is a significant difference in terms of the bottom depth at these three locations (DS: ~ 75 m; QMG: ~ 125 m; CG: ~ 325 m), as indicated by the different scales of the y -axis in these plots.

Both of Figs. 13 and 14 show that the surface layer at all locations exhibits significant seasonal variation. Due to ice melting and river discharge, the minimum salinity in DS and QMG can reach as low as ~ 15 psu in the summer, while the minimum salinity in CG can also drop to below 20 psu in certain years. The temperature of the surface layer varies from $\sim -2^\circ\text{C}$ in the winter to $\sim 6^\circ\text{C}$, $\sim 8^\circ\text{C}$ and $\sim 10^\circ\text{C}$ in QMG, DS and CG, respectively, in the summer. The seasonal variation is also evident in terms of the thickness of the surface layer. If we define the bottom of the surface layer by the 29 psu isopycnal, as indicated by the black contours in Fig. 13, then it is clear that the layer thickness varies from ~ 20 m by the end of the ice-covered season to over ~ 60 m by the end of the ice-free season. In late spring/early summer of each year when sea ice and river ice melts, freshwater enters the Kitikmeot Sea, decreasing the surface salinity. In the mean time, the surface temperature also increases due to direct solar radiation. Due to direct wind-driven mixing, the surface layer also deepens (Lincoln et al., 2016; Rainville, Lee, & Woodgate, 2011). The entire water column of DS can be well mixed by the end of the ice-free season, though this is not the case in CG and QMG due to the larger depth. The deepening of the surface layer stops in early winter (November) when sea ice forms again, which acts as a rigid lid that prevents direct wind-driven mixing of the surface layer, and the pycnocline shoals gradually due to the outflow of surface freshwater through DUS and VS.

The layer immediately below the surface layer extends to approximately 150 m of depth, which is below the bottom depth of DS and QMG. This layer has an average salinity of approximately 30 psu and an average temperature of 0°C , and it does not show significant seasonal

variation except for its upper boundary. In CG, there also exists a bottom layer, which has an average salinity of ~ 32.5 psu and an average temperature of -0.8°C , and is not influenced by the seasonal cycle of the surface layer. Mixing between the bottom and middle layers in CG is likely to be limited, since the pycnocline appears quiescent throughout the entire study period. The bottom waters could be from overflow of the saltier and denser water through DUS and VS, and are likely to consist of water from Pacific origin, given the close proximity of the Kitikmeot Sea to the Alaska coast and channels in the northern CAA which are a major pathway for Pacific water transport (Dmitrenko et al., 2018; Hu et al., 2019). Hence, the bottom water is likely to have relatively higher nutrient concentration, and thus is potentially important for the biogeochemical processes. The exact origin of the bottom water and the processes of deep water renewal and diapycnal mixing in the Kitikmeot Sea are beyond the scope of this paper but are a potential topic for future study.

The Hovmöller plots for density profiles are not shown, since the density in the Kitikmeot Sea is primarily determined by the salinity and the density plots appear almost identical to the salinity plots. Nevertheless, some quantitative measurements are given in Table 2. In particular, the table suggests that the minimum density can reach approximately 1011 kg/m^3 , while the average density of the middle layer is approximately 1022 kg/m^3 , implying the existence of strong stratification in the Kitikmeot Sea at least in the summer.

4.c *Circulation*

The ocean circulation of the Kitikmeot Sea is significantly influenced by seasonal ice coverage (and hence wind stress in the ice-free season) and the Earth's rotation. The seasonal variation of ocean currents can be seen in Fig. 15. Only the zonal component of the velocity field is shown, because the fact that the Kitikmeot Sea is an east–west waterway determines that the zonal component is dominant. Fig. 15 clearly shows that ocean current in the ice-free season is much stronger than that in the ice covered season. This is because without ice coverage, momentum input from wind stress can reach the ocean surface and affect the ocean circulation directly.

Compared to water bodies at a lower latitude, the Coriolis effect plays a more important role in the circulation of the Kitikmeot Sea and channels in the CAA in general. Nurser and Bacon (2014) showed that the Rossby radius of deformation of a typical channel within the CAA is approximately 6 km. The Kitikmeot Sea has a width of 20–50 km (the narrowest cross-section at Dease Strait is approximately 20 km), much larger than the deformation radius. Due to the Coriolis effect, flows to the east are along the south shore while flows to the west are along the north shore (see Fig. 6 of McLaughlin et al., 2004, for a detailed description of such mechanism). This flow pattern is not unique to the Kitikmeot Sea but also observed in other channels within the CAA (see, e.g., Fig. 3 of Hughes, Klymak, Hu, & Myers, 2017).

Unlike channels in the northern CAA in which the mean flow is generally southward and/or eastward, in the Kitikmeot Sea the flow direction is not consistent but exhibits significant variation that is related primarily to the wind stress, especially during the ice-free season when the flow is driven directly by the wind stress. To illustrate the relationship, a comparison of surface velocity from model output and wind stress from CGRF dataset in August of selected years is given in Fig. 16. The figure shows that northwest wind is dominant in 2012 and 2018 while southeast wind is dominant in 2015. As a result, surface current is also eastward in 2012 and 2018, and westward in 2015. Comparing between 2012 and 2018, the figure shows that when wind speed is faster, the surface current is also stronger. The surface current is also influenced by topographical features. As evident in panels (a) and (c), under northwest wind, strong current exists to the south of Finlayson Islands along the shore of Kent Peninsula. On the other hand, panel (b) shows that under southeast wind, flow is stronger along the north shore near Cambridge Bay. This is consistent with the flow pattern shown in Fig. 15, which suggests that time-averaged current is eastward along the south shore of the Dease Strait and westward along the north shore. When the wind direction is mainly northward or southward, the surface current does not have a preferred direction. Fig. 16 also shows that the Finlayson Islands in the middle of Dease Strait block and alter the flow to certain degree.

Before concluding this section, we would like to note that the tidal forcing, although not

included in the present model, is also expected to have non-negligible influence on the circulation of the Kitikmeot Sea, especially on a semi-diurnal to diurnal time scale. Since tidal currents are strong near the bounding sills at DUS and VS, they can significantly affect the inflow and outflow through these open boundaries, as well as the ice movement during the melting season. Future studies of the mixing in the Kitikmeot Sea should include explicit tidal forcing.

5 Discussion

The physical oceanographic conditions of the Kitikmeot Sea are different from channels in the northern CAA primarily due to the existence of a substantial ice-free period each year. Such ice conditions have several significant implications on both stratification and ocean circulation. During the ice-free season, external forcings such as ice melting, river discharge and solar radiation can act directly on the sea surface, leading to freshening and warming of the surface water. Our simulation results suggest that the minimum salinity in the Kitikmeot Sea can reach as low as 15 psu during the peak runoff season, while the minimum density can be close to 1010 kg/m^3 . In contrast, the average salinity and density of the bottom layer at CG are 32.5 psu and 1026 kg/m^3 , respectively, and do not show evidence of seasonal variation. Such a large salinity and density gradient implies the existence of a strong stratification in the Kitikmeot Sea, which significantly restricts the mixing between the surface and bottom water.

The annual variation of the freshwater storage in the Kitikmeot Sea, when combined from both the ocean and the sea ice, is slightly over 50 km^3 . The freshwater input during the melting season is due to net inflow of sea ice, runoff from land, and net precipitation, and is approximately balanced by the net outflow of freshwater during the freezing season. Quantitatively, the runoff contributes approximately 41 km^3 of freshwater each year (Williams et al., 2018) and is a major source of freshwater input, while the net inflow of sea ice through DUS and VS is approximately 14 km^3 per year. Being approximately $1/3$ of the total volume of runoff, the net inflow of sea ice is also a non-negligible source of the freshwater input. On the other hand, the contribution from

net precipitation is relatively minor, given that the average volume of freshwater input from the other two sources adds up to over 50 km^3 already.

As a result of differences in dynamic ice transport across the region, QMG is characterized by thicker ice, and lower summer surface salinity and temperature. Generally, ice melt and low surface temperatures drive low surface pCO_2 , while warmer surface temperatures drive higher pCO_2 . This spatial variation helps explain the biogeochemical observations of (Ahmed et al., 2019), who found that QMG typically acts as a sink for atmospheric CO_2 in the summer, while CG typically acts as a source of CO_2 to the atmosphere.

In the Arctic Ocean, inflow of water from the Pacific Ocean has been recognized as a dominant source of freshwater, heat and nutrients (Haine et al., 2015; Woodgate et al., 2010). Previous studies (e.g., Dmitrenko et al., 2018; Hu et al., 2019) showed that the Pacific water mainly follows the Transpolar Drift and is a major source of freshwater content in the Beaufort Gyre. Nevertheless, our simulation results suggest that the freshwater content per unit area in CG is larger than that in the Beaufort Gyre in general, due to the significant amount of ice melted and runoff from land relative to the small size of the Kitikmeot Sea. Our results also suggest that only the bottom water in CG has an average salinity that is similar to the salinity of the Pacific water, which varies seasonally from 31.9 psu to 33 psu (Woodgate, 2018). Thus, any Pacific water flowing into the Kitikmeot Sea is likely to sink to the bottom immediately, given its relatively higher density than the surface water in the Kitikmeot Sea. As a result, any nutrients brought into this region by the Pacific water are also likely to concentrate in the bottom layer due to the strong stratification and limited vertical mixing. This could be a potentially important reason why the Kitikmeot Sea has a low primary production and biological productivity (Back et al., 2021; Bouchard et al., 2018).

Another effect of the seasonal ice coverage is that, in the ice-free season, wind stress can force the ocean circulation directly. The direct momentum input from wind stress into the ocean leads to both wind-driven mixing and wind-driven circulation. The wind-driven mixing deepens the surface layer throughout the ice-free season. While the mixing is not strong enough to reach the

more nutrient-rich bottom layer, it still allows full mixing at locations where shallow sills exist such as DS, DUS and VS. As a result, the entire water column in these straits are well mixed. Therefore, direct wind-driven mixing can also lead to enhanced vertical mixing and potentially increase the biological productivity, in a way similar to the effect of tidal forcing (Dalman et al., 2019). To determine the relative importance of each of these mechanisms, a budget analysis should also include tidal mixing. It could be performed in future studies when the tidal forcing is included in the model.

The wind-driven circulation in the ice-free season leads to strong along-shore current whose speed can reach 0.1 m/s. This current speed is almost an order of magnitude larger than that in the ice-covered season, which is only approximately 0.01 m/s. The flow direction in the Kitikmeot Sea is not consistent, and is heavily influenced by the wind direction. In contrast, there exists strong southward/eastward mean flow in the northern CAA (McLaughlin et al., 2004), and the typical speed is on the order of 0.1 cm/s in most of the channels (Hughes et al., 2017). This implies that the ocean current in the Kitikmeot Sea is generally slow except when there exists strong wind in the ice-free season. This provides some support to the hypothesis that the near-absence of the Arctic cod in the Kitikmeot Sea is partially due to the fact that their larvae are not easily dispersed by the slow current (Bouchard et al., 2018).

While the present work focuses primarily on the seasonal variation of the physical oceanographic conditions of the Kitikmeot Sea, interannual variation is also evident, especially in the freshwater storage shown in Fig. 11. The increase of freshwater storage over the simulation period could be a consequence of climate change which leads to the freshening of the Arctic Ocean in general (McPhee et al., 2009). However, it might also be a short term trend, or even a model artifact due to possibly the lack of tidal forcing and hence inaccurate inflow/outflow conditions. Simulations of a much longer time span are needed to determine the existence of any systematic and long term impact of climate change on this region. Nevertheless, if the increase of freshwater storage and freshening of the surface layer is a result of climate change, then it is reasonable to assume that the stratification of the Kitikmeot Sea could be even stronger in the future,

such that the mixing efficiency and hence primary production would be further reduced. Further studies are needed to determine the implication of changing oceanographic conditions on the ecosystem and biogeochemistry in the Kitikmeot Sea.

6 Conclusions

In conclusion, the seasonal variation of the ice coverage leads to strong seasonal variation of the physical oceanographic conditions, including both stratification and circulation, of the Kitikmeot Sea. The seasonal variation of the stratification is characterized by the freshening of the surface layer through the melt of sea ice and runoff from land in the ice-free season, which significantly increases the strength of stratification and limits the vertical mixing. The circulation, on the other hand, is primarily driven by wind stress in the ice-free season, which leads to the deepening of surface layer and the increase of current speed, both of which increase the mixing efficiency at least for the surface layer. Nevertheless, given the short duration of the ice-free season and the large amount of freshwater input, the increase of mixing due to wind driven circulation is limited to only the surface layer and locations where shallow sills exist. For deep basins especially in CG, the bottom layer does not show evidence of any significant seasonal variation, and diapycnal mixing is limited throughout the year.

The model used in the present work has some limitations. For example, it has limited resolution, and a model with higher resolution would allow for more accurate and detailed analyses for future studies. For this reason, a higher-resolution model is under development, with the target resolution being $1/60^\circ$ in the horizontal directions. Another major limitation of the present model is the lack of tidal forcing, which is expected to play an important role in the inflow and outflow through the bounding sills at the open boundaries. With more accurate inflow and outflow data, we will be able to better quantify the budget of freshwater storage and the process of deep water renewal, both of which are essential for better understanding the mixing in this region, as well as the biological productivity and the entire ecosystem.

Acknowledgement

A portion of the data used in this work were provided by Ocean Networks Canada.

We thank the captain and crew of the RV Martin Bergmann for their assistance collecting the CTD validation data. We thank Mike Dempsey at Fisheries and Oceans Canada for annually calibrating the CTD rosette. Logistical support was provided by Polar Knowledge Canada, and the Arctic Research Foundation. Shawn Marriott and Francis Emingak assisted with field data collection. Special thanks to C.J. Mundy for his role in initiating and continuing the R/V Martin Bergmann cruises.

We thank the NEMO development team as well as the DRAKKAR group for providing the model code and continuous guidance. We express our thanks to Westgrid and Compute Canada (<http://www.computecanada.ca>) for the computational resources to carry out our numerical simulations as well as archival of the experiments.

Financial support was provided by the Marine Environmental Observation Prediction and Response (MEOPAR) network, the Natural Sciences and Engineering Research Council of Canada (NSERC), Irving Shipbuilding, and the ArcticNet network. The involvement of P.G.M. in this work was supported by an NSERC Climate Change and Atmospheric Research Grant (Grant RGPCC 433898) as well as an NSERC Discovery Grant (Grant RGPIN 04357). Q.Z. was supported in part by an NSERC Discovery Grant (Grant RGPIN-2018-04329).

We thank Charlene Feucher and Clark Pennelly for helping with the access and analysis of the ANHA12 model. We would also like to thank the two anonymous referees for their constructive comments and concrete suggestions that led to significant improvements of this work.

References

Ahmed, M., Else, B. G. T., Burgers, T. M., & Papakyriakou, T. (2019). Variability of surface water $p\text{CO}_2$ in the Canadian Arctic Archipelago from 2010 to 2016. *J. Geophys. Res. Oceans*, *124*, 1876–1896.

- Amante, C., & Eakins, B. W. (2009). ETOPO1 1 Arc-Minute Global Relief Model: Procedures, Data Sources and Analysis. In *NOAA Technical Memorandum NESDIS NGDC-24*. National Geophysical Data Center, NOAA.
- Back, D.-Y., Ha, S.-Y., Else, B., Hanson, M., Jones, S. F., Shin, K.-H., ... Mundy, C. J. (2021). On the impact of wastewater effluent on phytoplankton in the Arctic coastal zone: A case study in the Kitikmeot Sea of the Canadian Arctic. *Sci. Total Environ.*, *764*, 143861.
- Bamber, J., van den Broeke, M., Ettema, J., Lenaerts, J., & Rignot, E. (2012). Recent large increases in freshwater fluxes from Greenland into the North Atlantic. *Geophys. Res. Lett.*, *39*, L19501.
- Bernard, B., Madec, G., Penduff, T., Molines, J.-M., Treguier, A.-M., Le Sommer, J., ... De Cuevas, B. (2006). Impact of partial steps and momentum advection schemes in a global ocean circulation model at eddy-permitting resolution. *Ocean Dyn.*, *56*(5), 543–567.
- Bouchard, C., Geoffroy, M., LeBlanc, M., & Fortier, L. (2018). Larval and adult fish assemblages along the Northwest Passage: the shallow Kitikmeot and the ice-covered Parry Channel as potential barriers to dispersal. *Arct. Sci.*, *4*, 781–793.
- Dai, A., Qian, T., Trenberth, K. E., & Milliman, J. D. (2009). Changes in continental freshwater discharge from 1948 to 2004. *J. Clim.*, *22*(10), 2773–2792.
- Dalman, L., Else, B., Barber, D., Carmack, E., Williams, W., Campbell, K., ... Mundy, C. (2019). Enhanced bottom-ice biomass along a tidal strait in the Kitikmeot Sea of the Canadian Arctic. *Elem. Sci. Anth.*, *7*, 22.
- Dmitrenko, I. A., Kirillov, S. A., Myers, P. G., Forest, A., Tremblay, B., Lukovich, J. V., ... Barber, D. G. (2018). Wind-forced depth-dependent currents over the eastern Beaufort Sea continental slope: Implications for Pacific water transport. *Elem. Sci. Anth.*, *6*, 66.
- Drakkar Group. (2007). Eddy-permitting ocean circulation hindcasts of past decades. *CLIVAR Exchanges*, *12*(3), 8–10.
- Duke, P., Else, B., Jones, S., Marriott, S., Ahmed, M., Nandan, V., ... Thomas, H. (2021).

- Seasonal marine carbon system processes in an Arctic coastal landfast sea ice environment observed with an innovative underwater sensor platform. *Elem. Sci. Anth.*. (Accepted)
- Falardeau-Côté, M. (2020). *The Arctic Ocean under multiple pressures: Linking impacts on marine ecosystem processes, ecosystem services, and human well-being* (Unpublished doctoral dissertation). McGill University.
- Fichefet, T., & Maqueda, M. A. M. (1997). Sensitivity of a global sea ice model to the treatment of ice thermodynamics and dynamics. *J. Geophys. Res. Oceans*, *102*(C6), 12609–12646.
- Haas, C., & Howell, S. E. L. (2015). Ice thickness in the Northwest Passage. *Geophys. Res. Lett.*, *42*, 7673–7680.
- Haine, T. W. N., Curry, B., Gerdes, R., Hansen, E., Karcher, M., Lee, C., . . . Woodgate, R. (2015). Arctic freshwater export: Status, mechanisms, and prospects. *Global Planet. Change*, *125*, 13-35.
- Harris, L. N., Yurkowski, D. J., Gilbert, M. J. H., Else, B. G. T., Duke, P. J., Ahmed, M. M. M., . . . Moore, J.-S. (2020). Depth and temperature preference of anadromous Arctic char *Salvelinus alpinus* in the Kitikmeot Sea, a shallow and low-salinity area of the Canadian Arctic. *Mar. Ecol. Prog. Ser.*, *634*, 175–197.
- Howell, S. E. L., Derksen, C., Pizzolato, L., & Brady, M. (2015). Multiyear ice replenishment in the Canadian Arctic Archipelago: 1997-2013. *J. Geophys. Res. Oceans*, *120*, 1623-1637.
- Howell, S. E. L., Wohlleben, T., Dabboor, M., Derksen, C., Komarov, A., & Pizzolato, L. (2013). Recent changes in the exchange of sea ice between the Arctic Ocean and the Canadian Arctic Archipelago. *J. Geophys. Res. Oceans*, *118*, 3595–3607.
- Hu, X., Myers, P. G., & Lu, Y. (2019). Pacific Water pathway in the Arctic Ocean and Beaufort Gyre in two simulations with different horizontal resolutions. *J. Geophys. Res. Oceans*, *124*, 6414–6432.
- Hu, X., Sun, J., Chan, T. O., & Myers, P. G. (2018). Thermodynamic and dynamic ice thickness contributions in the Canadian Arctic Archipelago in NEMO-LIM2 numerical simulations. *Cryosphere*, *12*, 1233–1247.

- Hughes, H. G., Klymak, J. M., Hu, X., & Myers, P. G. (2017). Water mass modification and mixing rates in a $1/12^\circ$ simulation of the Canadian Arctic Archipelago. *J. Geophys. Res. Oceans*, *122*, 803–820.
- Hunke, E. C., & Dukowicz, J. K. (1997). An elastic-viscous-plastic model for sea ice dynamics. *J. Phys. Oceanogr.*, *27*, 1849–1867.
- Lincoln, B. J., Rippeth, T. P., Lenn, Y.-D., Timmermans, M. L., Williams, W. J., & Bacon, S. (2016). Wind-driven mixing at intermediate depths in an ice-free Arctic Ocean. *Geophys. Res. Lett.*, *43*, 9749–9756.
- Madec, G., & the NEMO team. (2008). NEMO ocean engine. In *Scientific Notes of Climate Modelling Center (27)*. Institut Pierre-Simon Laplace (IPSL).
- Masina, S., Storto, A., Ferry, N., Valdivieso, M., Haines, K., Balmaseda, M., ... Parent, L. (2017). An ensemble of eddy-permitting global ocean reanalyses from the MyOcean project. *Clim. Dyn.*, *49*(3), 813–841.
- McLaughlin, F. A., Carmack, E. C., Ingram, R. G., Williams, W. J., & Michel, C. (2004). Oceanography of the Northwest Passage. In A. R. Robinson & K. H. Brink (Eds.), *The sea* (Vol. 14, pp. 1211–1242). Harvard University Press.
- McPhee, M. G., Proshutinsky, A., Morison, J. H., Steele, M., & Alkire, M. B. (2009). Rapid change in freshwater content of the Arctic Ocean. *Geophys. Res. Lett.*, *36*, L10602.
- Michel, C., Hamilton, J., Hansen, E., Barber, D., Reistad, M., Iacozza, J., ... Niemi, A. (2015). Arctic Ocean outflow shelves in the changing Arctic: A review and perspectives. *Prog. Oceanogr.*, *139*, 66–88.
- Myers, P. G., & Ribergaard, M. H. (2013). Warming of the polar water layer in Disko Bay and potential impact on Jakobshavn Isbrae. *J. Phys. Oceanogr.*, *43*, 2629–2640.
- Nurser, A., & Bacon, S. (2014). The Rossby radius in the Arctic Ocean. *Ocean Sci.*, *10*, 967–975.
- Padman, L., & Erofeeva, S. (2004). A barotropic inverse tidal model for the Arctic Ocean. *Geophys. Res. Lett.*, *31*, L02303.

- Proshutinsky, A., Krishfield, R., Toole, J. M., Timmermans, M., Williams, W., Zimmermann, S., ... Zhao, J. (2019). Analysis of the Beaufort Gyre freshwater content in 2003–2018. *J. Geophys. Res. Oceans*, *124*, 9658–9689.
- Rainville, L., Lee, C. M., & Woodgate, R. A. (2011). Impact of wind-driven mixing in the Arctic Ocean. *Oceanography*, *24*, 136–145.
- Shimada, K., Kamoshida, T., Itoh, M., Nishino, S., Carmack, E., McLaughlin, F., ... Proshutinsky, A. (2006). Pacific Ocean inflow: Influence on catastrophic reduction of sea ice cover in the Arctic Ocean. *Geophys. Res. Lett.*, *33*, L08605.
- Smith, G. C., Roy, F., Mann, P., Dupont, F., Brasnett, B., Lemieux, J.-F., ... Bélair, S. (2014). A new atmospheric dataset for forcing ice–ocean models: Evaluation of reforecasts using the Canadian global deterministic prediction system. *Q. J. R. Meteorol. Soc.*, *140*(680), 881–894.
- Smith, W. H., & Sandwell, D. T. (1997). Global sea floor topography from satellite altimetry and ship depth soundings. *Sci.*, *277*(5334), 1956–1962.
- Timco, G. W., & Frederking, R. M. W. (1996). A review of sea ice density. *Cold Reg. Sci. Technol.*, *24*, 1–6.
- Williams, W., Brown, K., Bluhm, B., Carmack, E., Dalman, L., Danielson, S., ... Schimnowski, A. (2018). Stratification in the Canadian Arctic Archipelago’s Kitikmeot Sea: Biological and geochemical consequences. In *2018 Polar Knowledge: Aqhaliat Report* (pp. 46–52). Polar Knowledge Canada.
- Woodgate, R. A. (2018). Increases in the Pacific inflow to the Arctic from 1990 to 2015, and insights into seasonal trends and driving mechanisms from year-round Bering Strait mooring data. *Prog. Oceanogr.*, *160*, 124–154.
- Woodgate, R. A., Aagaard, K., & Weingartner, T. J. (2006). Interannual changes in the Bering Strait fluxes of volume, heat and freshwater between 1991 and 2004. *Geophys. Res. Lett.*, *33*, L15609.
- Woodgate, R. A., Weingartner, T. J., & Lindsay, R. W. (2010). The 2007 Bering Strait oceanic

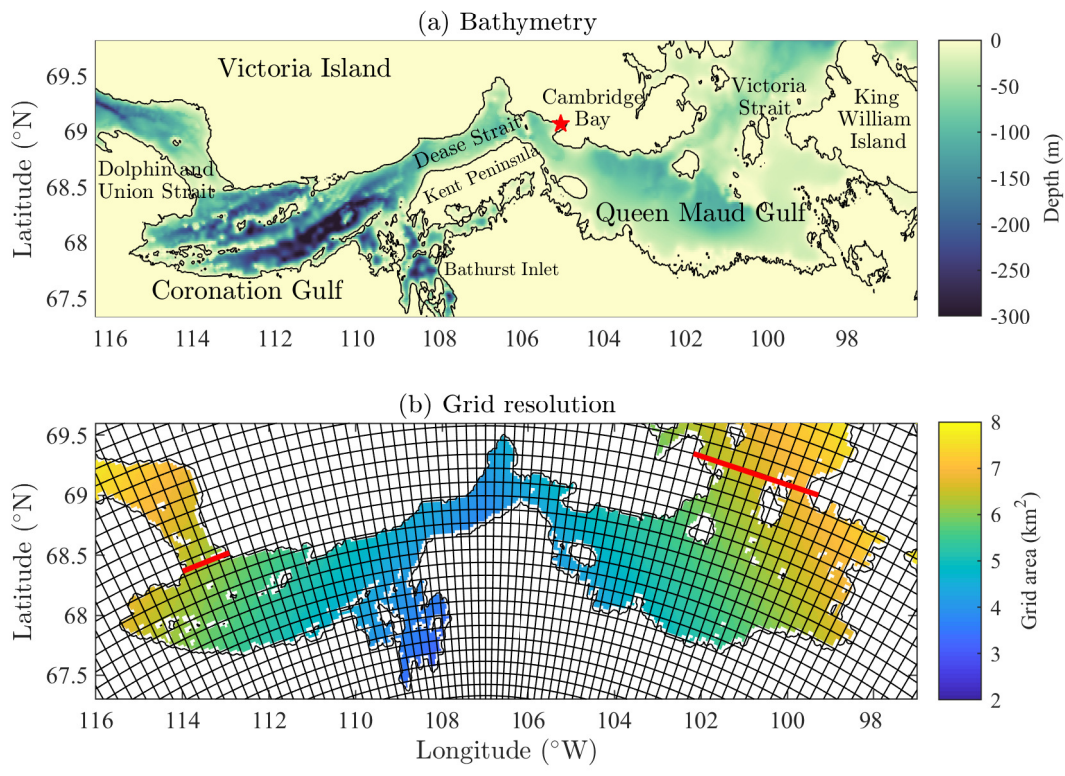


Fig. 1 (a) Bathymetry map of the Kitikmeot Sea. (b) ANHA12 grid resolution in the Kitikmeot Sea. Pseudo-color map shows the area covered by each horizontal grid box. Mesh grid shows the distribution of every five horizontal grid points. Red lines in Panel (b) indicate the two open boundaries of the Kitikmeot Sea.

heat flux and anomalous Arctic sea-ice retreat. *Geophys. Res. Lett.*, 37, L01602.

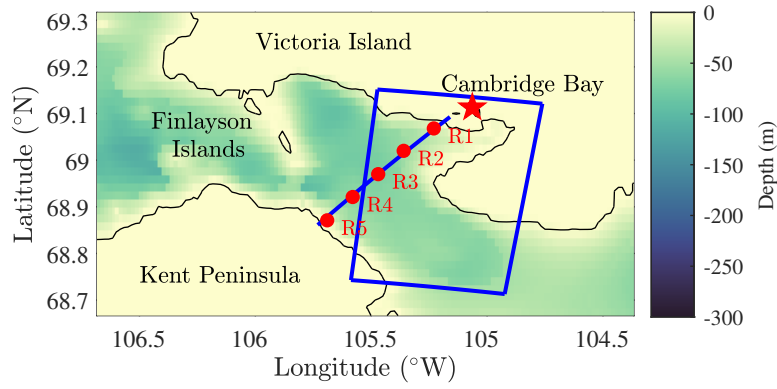


Fig. 2 Bathymetry map of Dease Strait and the Cambridge Bay area. The blue box indicates the area over which the model output is averaged for comparing with data collected by ONC’s cabled underwater observatory, whose location is indicated by the star (at Cambridge Bay). The red dots labeled as “R1” to “R5” indicate locations of CTD measurements on RV *Martin Bergmann*, while the blue line that connects these locations indicates the R-transect.

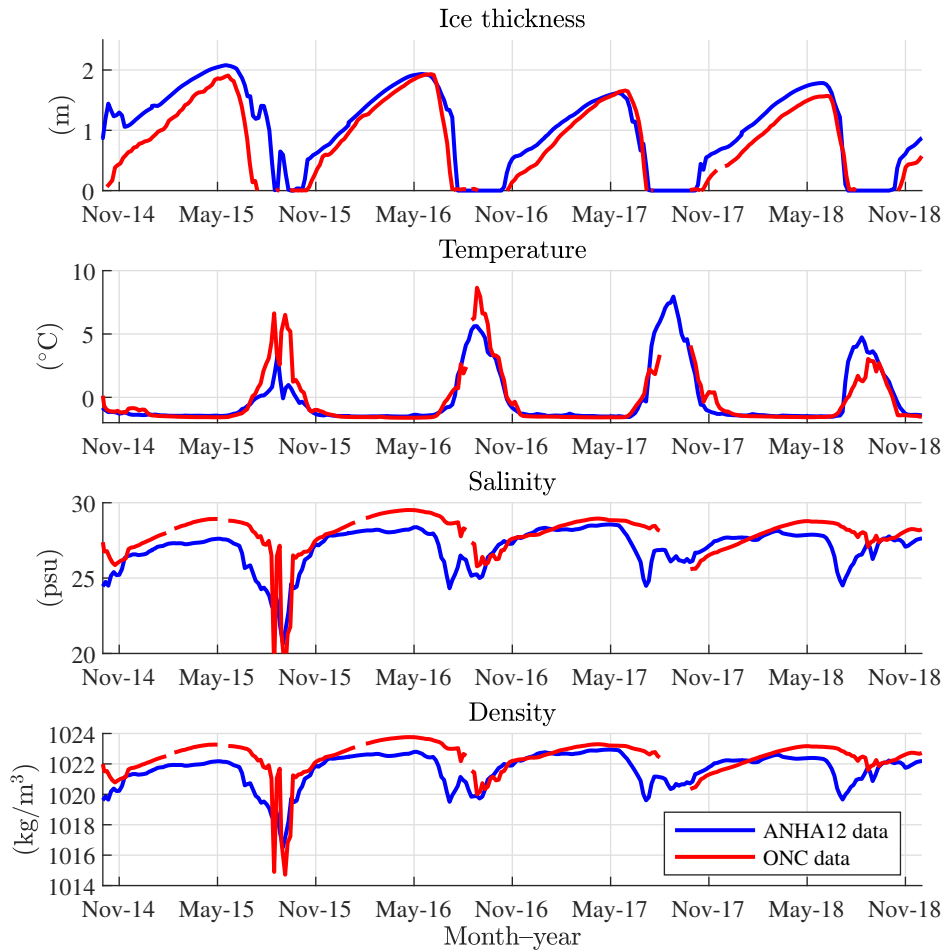


Fig. 3 Time series of (a) ice thickness, (b) temperature (c) salinity and (d) density from November 2014 to November 2018 in the Cambridge Bay area at the depth of 8 m. Blue curves show data from the ANHA12 model, and red curves show data from ONC measurements. In panel (a), only the ice draft is reported by ONC. The ice thickness shown in the plot is estimated by 1.11 times of the ice draft, assuming that the density of ice is roughly 90% of the density of seawater.

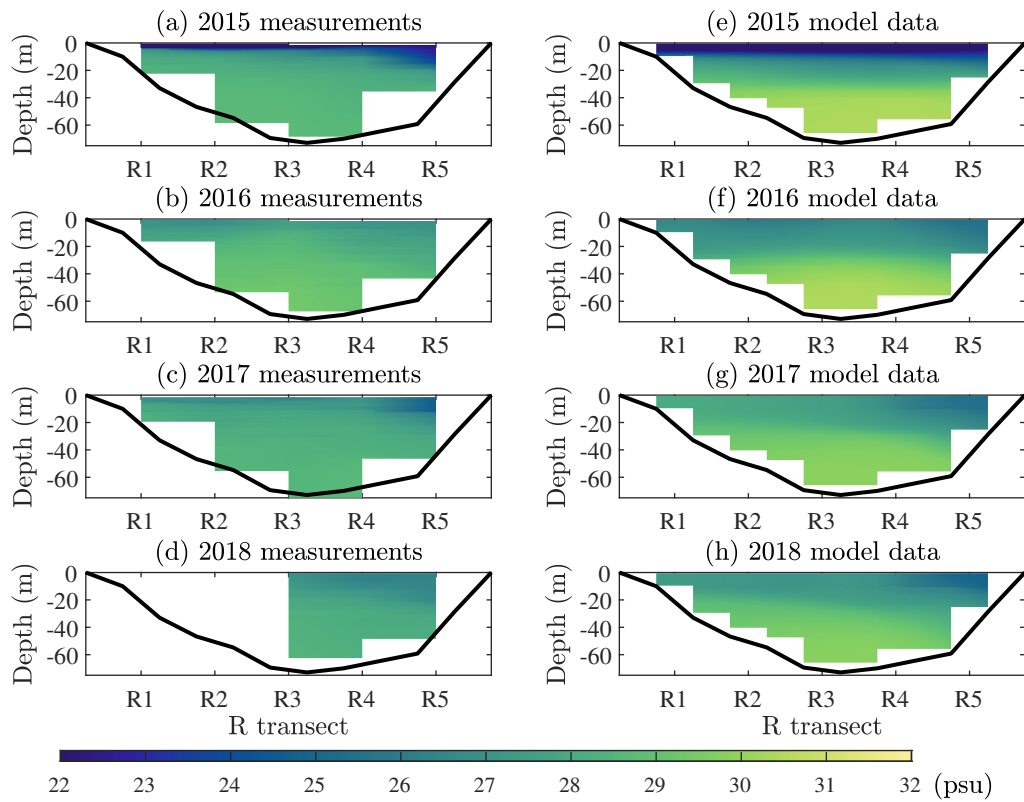


Fig. 4 (a)–(d) Salinity measured from RV Bergmann across the R-transect as shown in Fig. 2 in early August of 2015–2018. (e)–(h) Corresponding salinity data from output of the ANHA12 model. The model data are averaged over a 5-day period. Black curves indicate the approximate location of the ocean bottom. Note that the observational data for 2018 are incomplete for technical reasons.

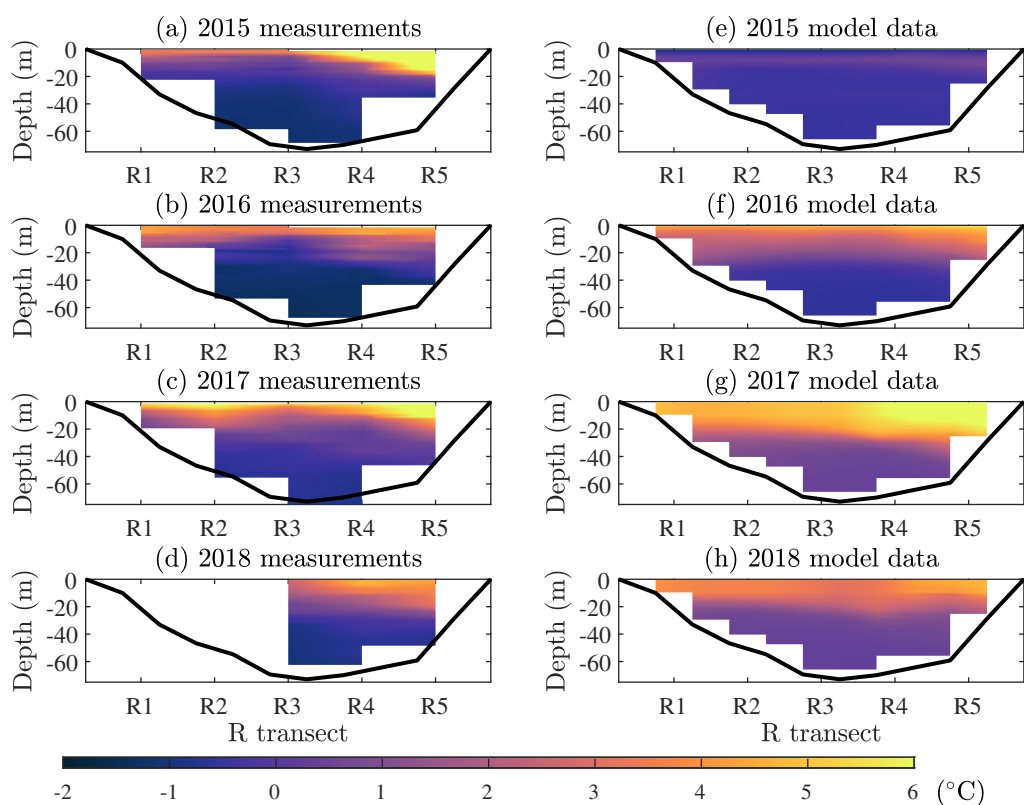


Fig. 5 Same as Fig. 4 but for temperature.

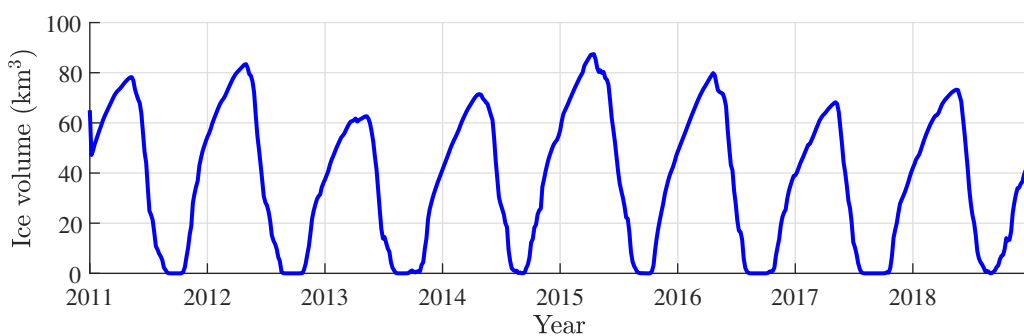


Fig. 6 Time series of ice volume within the Kitikmeot Sea from 2011 to 2018.

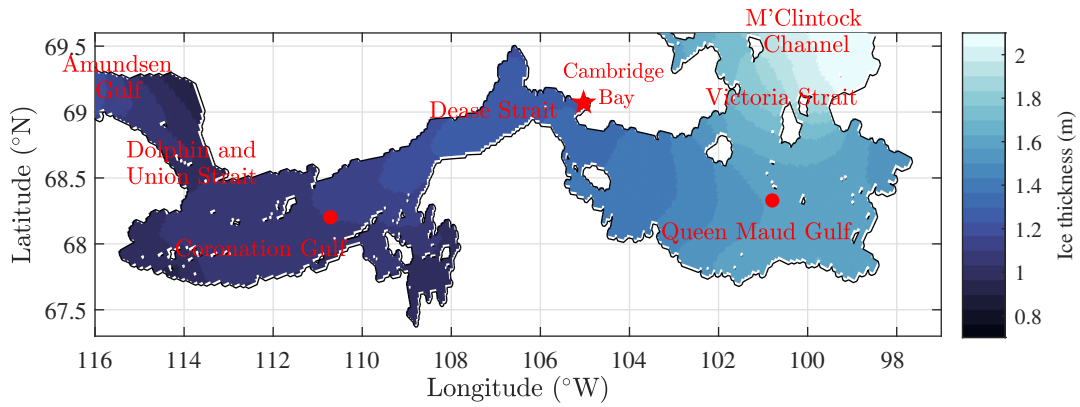


Fig. 7 Average ice thickness in the Kitikmeot Sea from November to June (averaged from 2011 to 2018). Red dots indicate locations within Coronation Gulf and Queen Maud Gulf at which time series in Fig. 8 are produced.

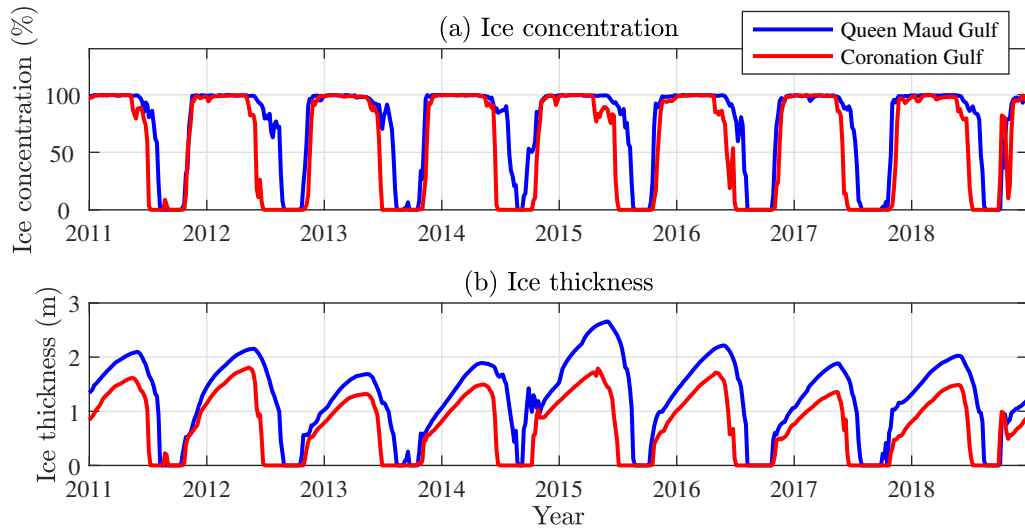


Fig. 8 Time series of (a) ice concentration and (b) ice thickness of Coronation Gulf (red) and Queen Maud Gulf (blue) from 2011 to 2018. The particular locations at which the time series are produced are indicated by the red dots in Fig. 7.

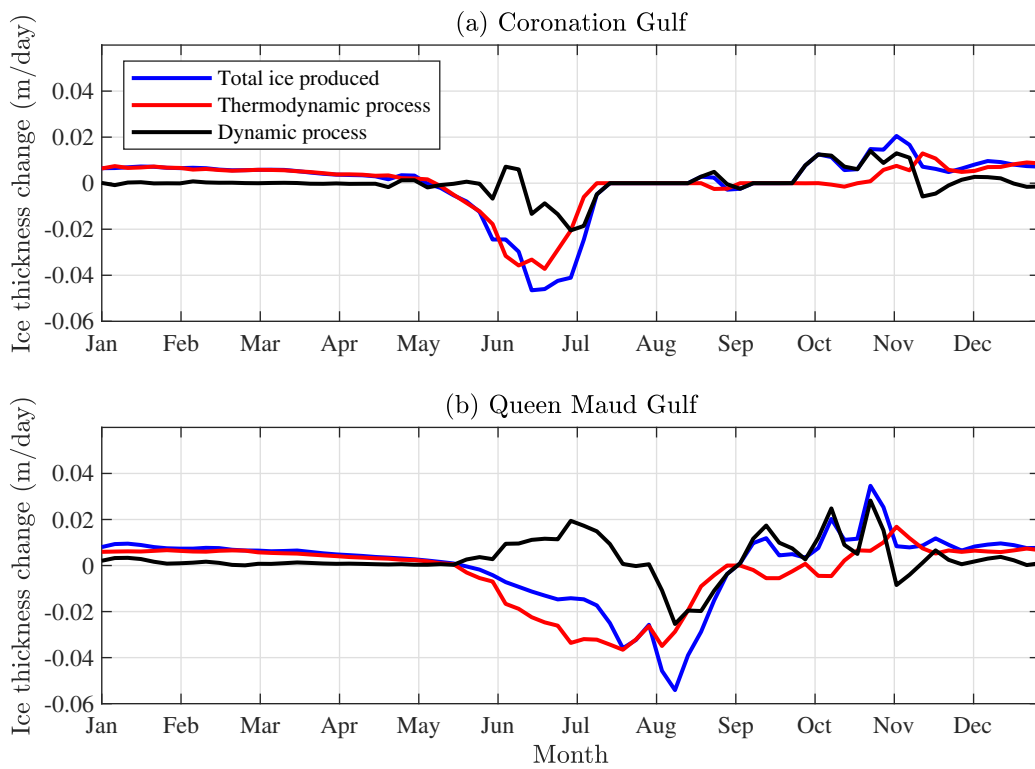


Fig. 9 Seasonal cycle (averaged from 2011 to 2018) of overall ice thickness changes (blue), and ice thickness changes due to thermodynamic (red) and dynamic (black) processes at (a) Coronation Gulf and (b) Queen Maud Gulf. The particular locations at which the time series are produced are indicated by the red dots in Fig. 7.

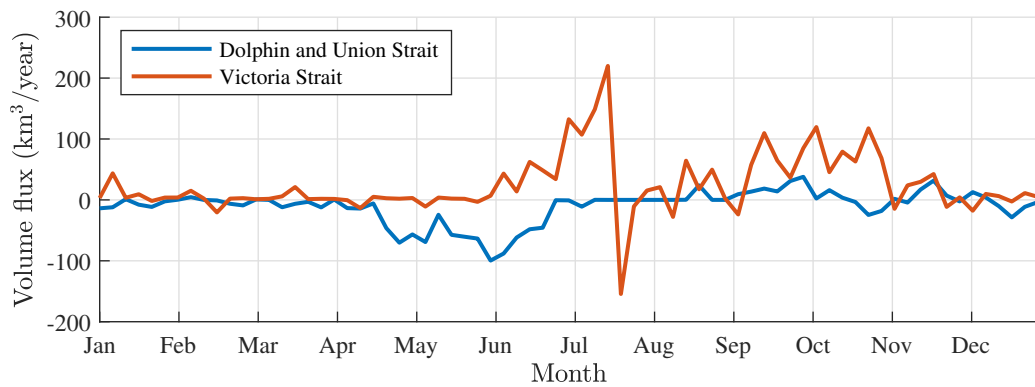


Fig. 10 Seasonal cycle (averaged from 2011 to 2018) of net inflow of sea ice through Dolphin and Union Strait (blue) and Victoria Strait (orange).

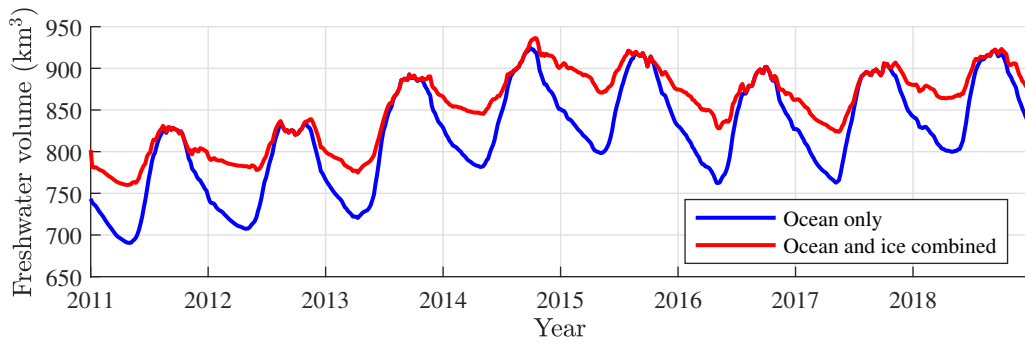


Fig. 11 Time series of freshwater storage in the Kitikmeot Sea from 2011 to 2018. Blue: freshwater storage in the ocean only; red: freshwater storage in the ocean and sea ice combined. The freshwater storage in the ocean is calculated based on the reference salinity $S_{ref} = 34.8$ psu, while the freshwater storage in the ice is approximated by 0.9 times the ice volume.

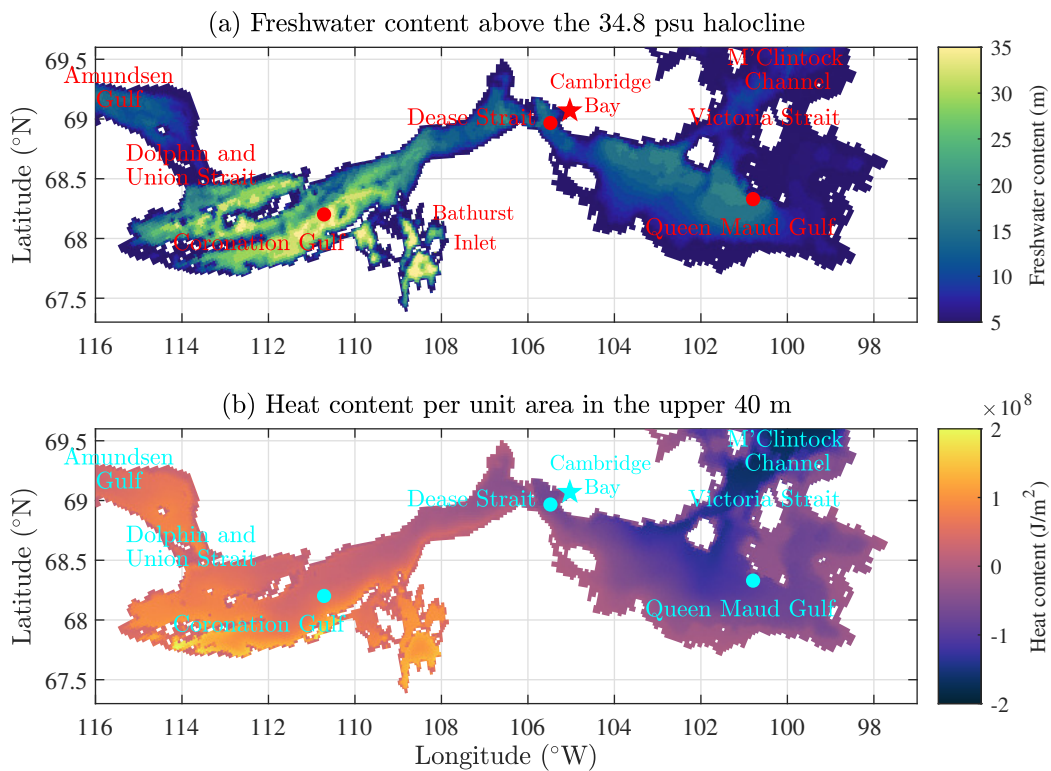


Fig. 12 (a) Freshwater content above the 34.8 psu halocline and (b) heat content per unit area in the upper 40 m, averaged from 2011 to 2018. Red/cyan dots indicate locations within Dease Strait, QMG and CG at which Hovmöller plots in Figs. 13–14 are produced.

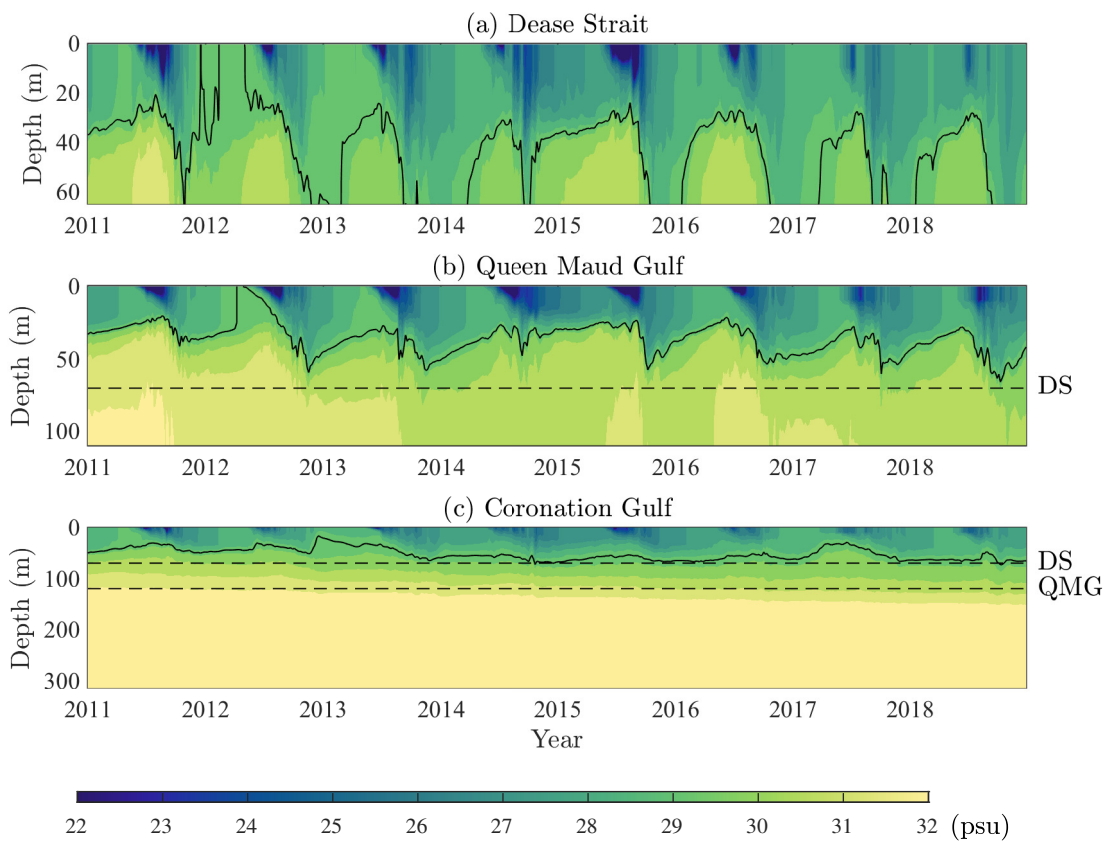


Fig. 13 Hovmöler plots of salinity at (a) Dease Strait, (b) Queen Maud Gulf and (c) Coronation Gulf as a function of time and depth from 2011 to 2018. The black contours indicate the depth of the 29 psu halocline. The particular locations at which the Hovmöler plots are produced are indicated by the red/cyan dots in Fig. 12. Note the different scales of the y -axis (depth) for each plot (location). The bottoms of Dease Strait (DS) and Queen Maud Gulf (QMG) are indicated by the dashed lines in panels (b) and (c).

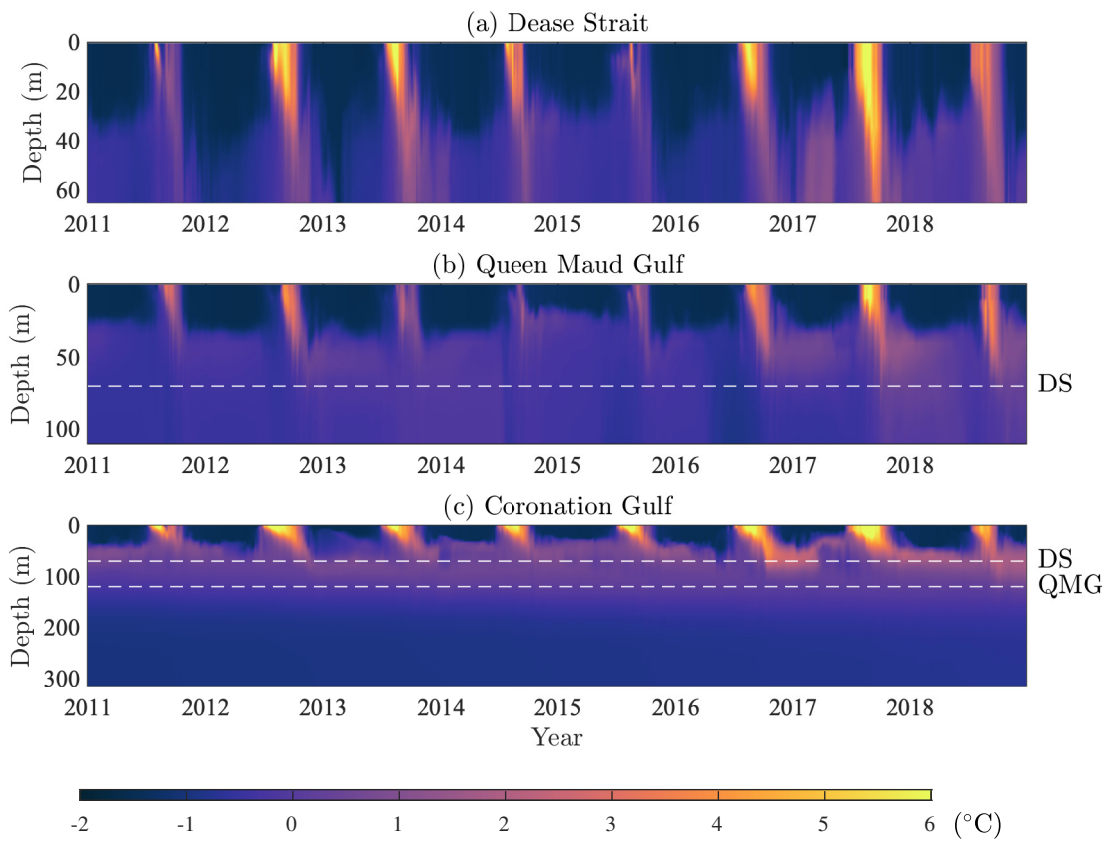


Fig. 14 Same as Fig. 13 but for temperature.

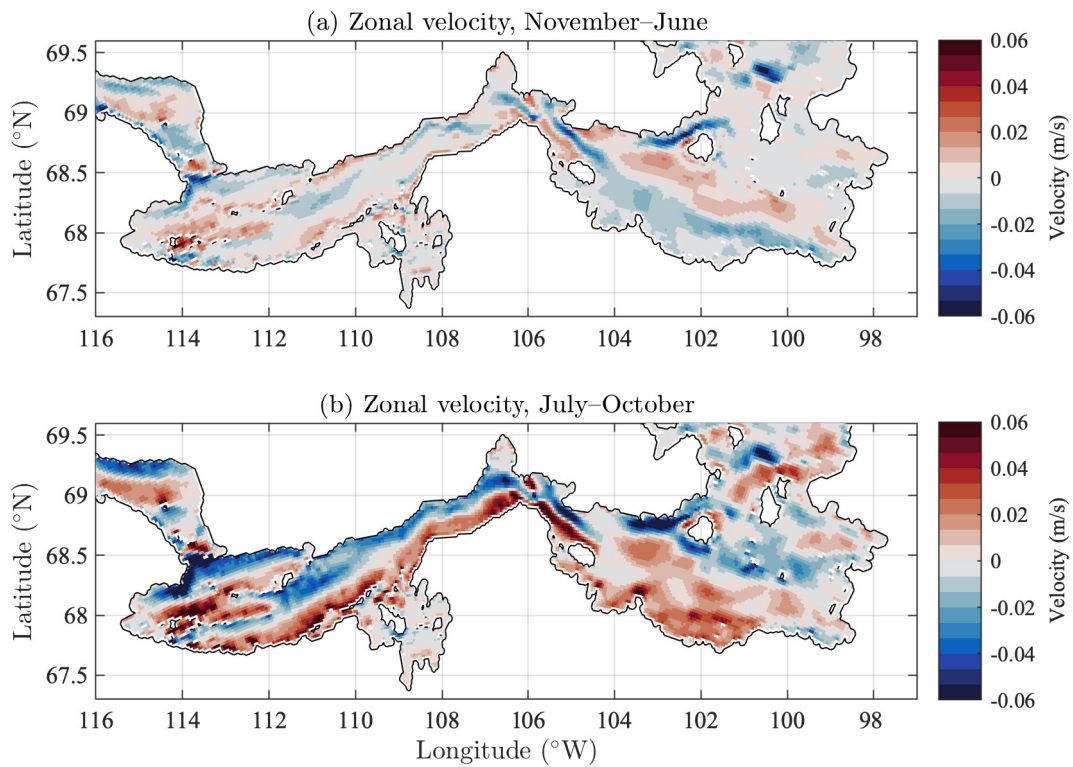


Fig. 15 Time and depth averaged zonal velocity of the Kitikmeot Sea from 2011 to 2018. (a) Ice-covered season: November–June. (b) Ice-free season: July–October. Positive velocity (red) is eastward, and negative velocity (blue) is westward.

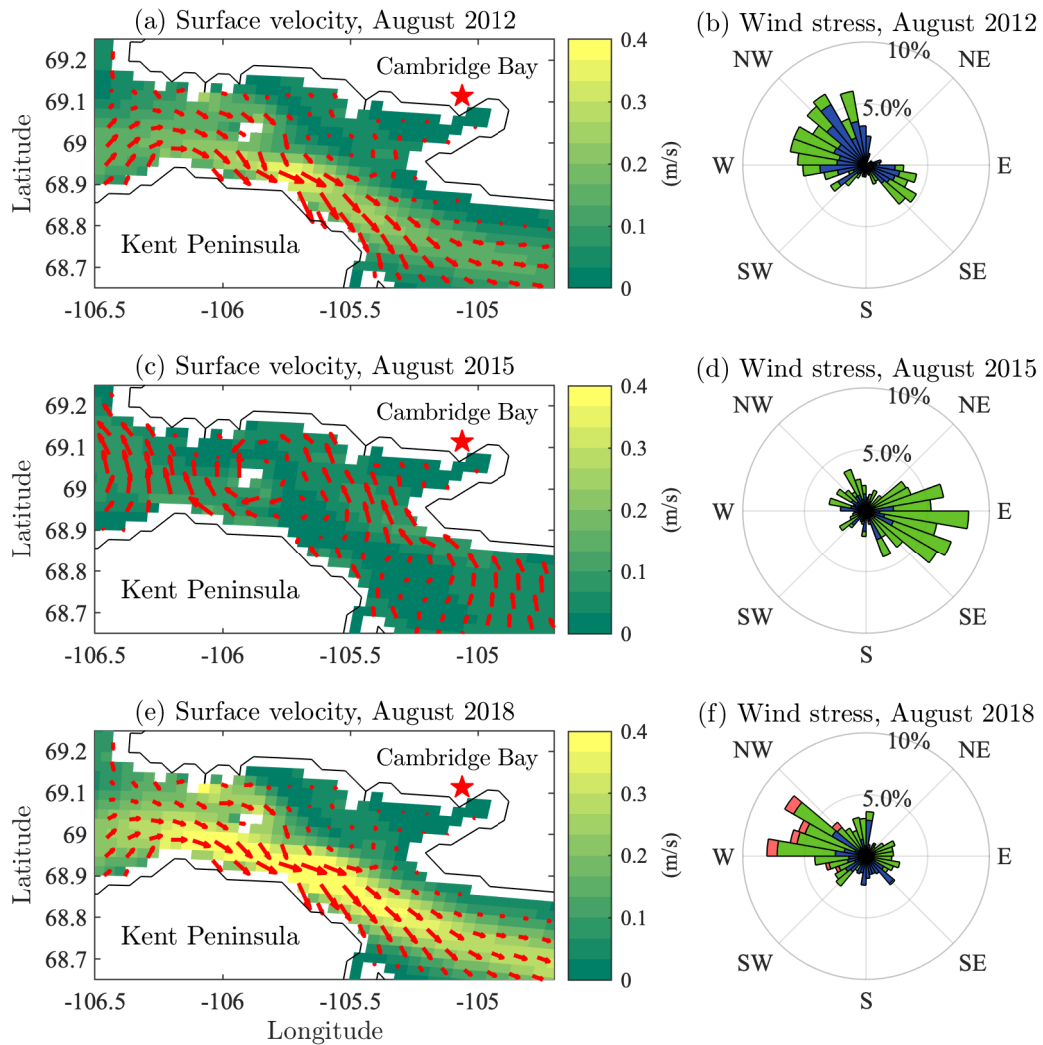


Fig. 16 (a,c,e) Time-averaged surface velocity near Cambridge Bay for August of 2012, 2015 and 2018. Pseudo-color map and arrows show the speed and direction of the surface current. (b,d,f) Distribution of hourly wind data from the CGRF dataset for August of 2012, 2015 and 2018. The data are averaged over the region of 104–108°W and 68.25–69.45°N. Blue, green and red in each bin of the wind rose diagram indicate wind speed of 0–5 m/s, 5–10 m/s and over 10 m/s, respectively. The length of each of the bins indicates the percentage of the hourly wind data from the corresponding direction.